J|A|C|S ARTICLES

Published on Web 08/11/2009

Direct Spectroscopic Observation of Large Quenching of First-Order Orbital Angular Momentum with Bending in Monomeric, Two-Coordinate Fe(II) Primary Amido Complexes and the Profound Magnetic Effects of the Absence of Jahn−and Renner−Teller Distortions in Rigorously Linear Coordination

W. Alexander Merrill,[†] Troy A. Stich,[†] Marcin Brynda,[†] Gregory J. Yeagle,[†] James C. Fettinger,[†] Raymond De Hont,[¶] William M. Reiff,*[,‡] Charles E. Schulz,[§] R. David Britt,[†] and Philip P. Power*[,†]

Department of Chemistry, University of California, Davis, One Shields Avenue, Davis, California 95616, Department of Chemistry and Chemical Biology, Northeastern University, 360 Huntington Avenue, Boston, Massachusetts 02115, Marine Science Research Center, Northeastern University, 430 Nahant Road, Nahant, Massachusetts, 01908, Department of Chemistry, Carnegie Mellon University, 4400 Fifth Avenue, Pittsburgh, Pennsylvania 15213, and Department of Physics, Knox College, Galesburg, Illinois 61401

Received April 28, 2009; E-mail: pppower@ucdavis.edu; w.reiff@neu.edu

Abstract: The monomeric iron(II) amido derivatives Fe{N(H)Ar*}$_2$ (**1**), Ar* = C_6H_3-2,6-(C_6H_2-2,4,6-Pr^i_3)$_2$, and Fe{N(H)Ar$^{\#}$}$_2$ (**2**), Ar$^{\#}$ = C_6H_3-2,6-(C_6H_2-2,4,6-Me_3)$_2$, were synthesized and studied in order to determine the effects of geometric changes on their unusual magnetic properties. The compounds, which are the first stable homoleptic primary amides of iron(II), were obtained by the transamination of Fe{N(SiMe$_3$)$_2$}$_2$, with HN(SiMe$_3$)$_2$ elimination, by the primary amines H_2NAr* or H_2NAr$^{\#}$. X-ray crystallography showed that they have either strictly linear (**1**) or bent (**2**, N−Fe−*N* = 140.9(2)°) iron coordination. Variable temperature magnetization and applied magnetic field Mössbauer spectroscopy studies revealed a very large dependence of the magnetic properties on the metal coordination geometry. At ambient temperature, the linear **1** displayed an effective magnetic moment in the range 7.0−7.50 μ_B, consistent with essentially free ion magnetism. There is a very high internal orbital field component, $H_L \approx 170$ T which is only exceeded by a $H_L \approx 203$ T of Fe{C(SiMe$_3$)$_3$}$_2$. In contrast, the strongly bent **2** displayed a significantly lower μ_{eff} value in the range 5.25−5.80 μ_B at ambient temperature and a much lower orbital field H_L value of 116 T. The data for the two amido complexes demonstrate a very large quenching of the orbital magnetic moment upon bending the linear geometry. In addition, a strong correlation of H_L with overall formal symmetry is confirmed. ESR spectroscopy supports the existence of large orbital magnetic moments in **1** and **2**, and DFT calculations provide good agreement with the physical data.

Introduction

Although the gas-phase electron diffraction structure of the linear d^5 species Mn(CH$_2$Bu^t)$_2$ was reported over three decades ago,[1] the synthesis and X-ray structure of Mn{C(SiMe$_3$)$_3$}$_2$ in 1985 marked the first determination of the structure of a stable, open shell, two-coordinate molecular transition metal species in the solid state.[2] Since then the half-filled shell manganese(II) species have been joined by several other two-coordinate d^5 derivatives, and the range of open-shell first row transition metal complexes has been extended to complexes with d^4, d^6, d^7, and d^8 electron configurations.[3,4] These include derivatives of Cr(I),[5] Cr(II),[5−8a] Mn(II),[1,2,7−11,13−15] Fe(II),[7,8a,10−12,14,21] Co(II),[7,8a,10,11,15,17] and Ni(II),[6−8] which all possess a high-spin electron configu-

[†] University of California, Davis.
[¶] Carnegie Mellon University.
[‡] Northeastern University.
[§] Knox College.

(1) Andersen, R. A.; Carmona-Guzman, E.; Gibson, J. F.; Wilkinson, G. *J. Chem. Soc., Dalton Trans.* **1976**, 2204.
(2) Buttrus, N. H.; Eaborn, C.; Hitchcock, P. B.; Smth, J. D.; Sullivan, A. C. *Chem. Commun.* **1985**, 1380.
(3) Power, P. P. *Comments Inorg. Chem.* **1989**, *8*, 177.
(4) Power, P. P. *Chemtracts Inorg. Chem.* **1994**, *6*, 181.
(5) Wolf, R.; Brynda, M.; Ni, C.; Long, G. J.; Power, P. P. *J. Am. Chem. Soc.* **2007**, *129*, 6076.
(6) Bartlett, R. A.; Chen, H.; Power, P. P. *Angew. Chem., Int. Ed.* **1989**, *28*, 316.
(7) Chen, H.; Bartlett, R. A.; Olmstead, M. M.; Power, P. P.; Shoner, S. C. *J. Am. Chem. Soc.* **1990**, *112*, 1048.
(8) (a) Nguyen, T.; Panda, A.; Olmstead, M. M.; Richards, A. F.; Stender, M.; Brynda, M.; Power, P. P. *J. Am. Chem. Soc.* **2005**, *127*, 8545. (b) Li, J.; Song, H.; Cui, C.; Cheng, J.-P. *Inorg. Chem.* **2008**, *47*, 3468.
(9) Andersen, R. A.; Berg, D. J.; Fernhold, L.; Faegri, K.; Green, J. C.; Haaland, A.; Leung, W.-P.; Rypdal, K. *Acta Chem. Scand.* **1988**, *42a*, 554.
(10) (a) Andersen, R. A.; Faegri, K.; Green, J. C.; Haaland, A.; Lappert, M. F.; Leung, W. P.; Rypdal, K. *Inorg. Chem.* **1988**, *27*, 1782. (b) Olmstead, M. M.; Power, P. P.; Shoner, S. C. *Inorg. Chem.* **1991**, *30*, 2547.

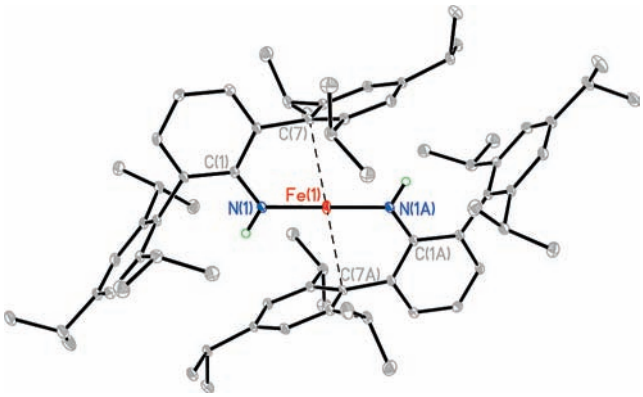

Figure 1. Thermal ellipsoid (30%) drawing of **1**. Hydrogen atoms (except N−H) are not shown. Fe---C(7),C(7)A 2.792 Å. Dashed lines indicate possible, very weak intramolecular interactions.

ration. Investigations of the magnetic properties of the rigorously linear Fe{C(SiMe$_3$)$_3$}$_2$ have shown that it exhibits essentially free ion magnetic behavior ($\mu_{eff} = 6.8 \pm 0.2\ \mu_B$) and the largest internal hyperfine fields (152 T) observed to date.[19,20] In addition, it has been shown that the almost linear Fe(NBu$^t_2$)$_2$ (N−Fe−N = 179.45(8)°) also possesses a high magnetic moment ($\mu_{eff} = 5.55\ \mu_B$) and a large internal hyperfine field (105 T). However, there have been no studies on two-coordinate species that feature different geometries with the same ligand class. Such a study provides a rare opportunity to investigate the effects of lowering the symmetry of the two-coordinate iron environment on the orbital contribution to the magnetic moment and internal hyperfine field while maintaining a very similar ligand set.

We report the synthesis of the closely related iron(II) amido complexes Fe{N(H)Ar*}$_2$ (**1**) (Ar* = C$_6$H$_3$-2,6-(C$_6$H$_2$-2,4,6-Pr$^i_2$)$_2$) and Fe{N(H)Ar$^\#$}$_2$ (**2**) (Ar$^\#$ = C$_6$H$_3$-2,6-(C$_6$H$_2$-2,4,6-Me$_3$)$_2$). They were characterized by X-ray crystallography, magnetization, zero- and applied field Mössbauer effect, and ESR spectroscopy and DFT calculations. The complexes possess local $D_{\infty h}$ (**1**), Figure 1, and C_{2v} (**2**), Figure 2, symmetry at iron. We show that the symmetry change from strict linearity induces dramatic effects on the magnetic properties of **2**.

Experimental Section

Synthetic Methods, Physical Measurements, and Calculations. General Procedures. All manipulations were performed with the use of modified Schlenk techniques under argon or in a Vacuum Atmospheres drybox under N$_2$. Solvents were dried and collected using a Grubbs-type[22] solvent purification system or distilled from Na/K alloy, and degassed by sparging with dry argon for 10 min. Ar$^\#$NH$_2$ was prepared from reduction of Ar$^\#$N$_3$ with LiAlH$_4$ in Et$_2$O,[23,24] Ar$^\#$N$_3$ having been prepared by treating Ar$^\#$Li[25] with *p*-toluenesulfonyl azide[26] in Et$_2$O. Ar*NH$_2$ was prepared in an analogous manner. Fe{N(SiMe$_3$)$_2$}$_2$ was synthesized according to a modified literature procedure,[10a] using anhydrous FeCl$_2$ (FeCl$_2$·4H$_2$O, Alfa, dehydrated at ∼250 °C under reduced pressure for 1 d) instead of the bromide. All physical measurements were obtained under strictly anaerobic conditions. ^{1}H NMR spectra were recorded on a Varian 300 MHz instrument and referenced internally to residual silicone vacuum grease, δ 0.29 ppm in C$_6$D$_6$. IR spectra were recorded as Nujol mulls between CsI plates on a Perkin-Elmer 1430 spectrophotometer. UV−vis spectra were recorded as dilute hexane solutions in 3.5 mL quartz cuvettes using a HP 8452 diode array spectrophotometer. Melting points were determined on a Meltemp II apparatus using glass capillaries sealed with vacuum grease and are uncorrected.

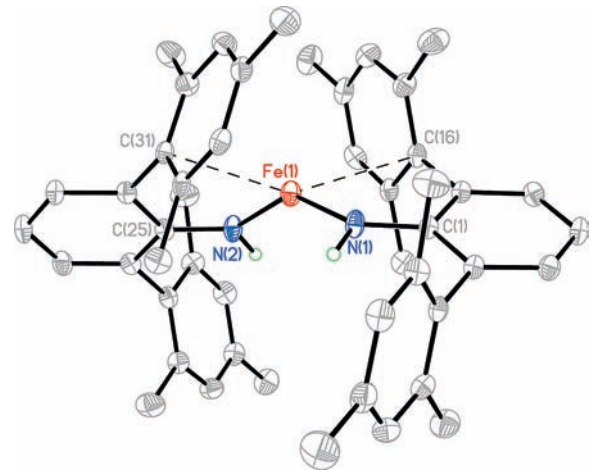

Figure 2. Thermal ellipsoid (30%) drawing of **2**. Hydrogen atoms (except N−H) are not shown. Fe(1)---C(16) 2.690 Å, Fe(1)---C(31) 2.588 Å. Dashed lines indicate weak intramolecular aryl π---Fe interactions.

Fe{N(H)Ar*}$_2$ (1). A Schlenk flask was charged with Ar*NH$_2$ (1.403 g, 3.0 mmol), Fe{N(SiMe$_3$)$_2$}$_2$ (0.678 g, 1.8 mmol), and a stirring bar. The mixture was then shaken as it was heated to ∼200 °C, melting and codissolving as the reaction ensued. Intermittent vacuum was applied over ∼10 min to remove the HN(SiMe$_3$)$_2$ byproduct as a white vapor. A deep-red solid resulted, and under reduced pressure, the entire flask was heated from bottom to top at ∼180 °C for 5 min to to complete the reaction, removing all the HN(SiMe$_3$)$_2$ as well as unreacted Fe{N(SiMe$_3$)$_2$}$_2$. The resulting solid was extracted with 40 mL of hexane, filtered on a medium frit with Celite, and concentrated to ∼15 mL. After 2 d standing at ∼25 °C deep-red, rod-shaped crystals appeared, yield 0.350 g (22%), mp 263 °C. ^{1}H NMR (300 MHz, C$_6$D$_6$, 25 °C) δ 7.09 (br, s, ArH), 1.21 (br, m), 0.84 (br, s), 0.19 (br, m), −13.2 (br, s), −57.2 (br, s). IR, cm^{-1}: ν(N−H) 3350; ν(Fe−N) 400. UV−vis, nm (ε, M^{-1} cm^{-1}): 450 (2840), 424 sh (2360), 320 (12100), 310 sh (11800).

Fe{N(H)Ar$^\#$}$_2$ (2). A Schlenk flask was charged with Ar$^\#$NH$_2$ (0.988 g, 3.0 mmol) and [Fe{N(SiMe$_3$)$_2$}$_2$] (0.678 g, 1.8 mmol), and a stirring bar. As the solids began reacting at ∼25 °C (indicated by a reddening of the crystalline Ar$^\#$NH$_2$), toluene (∼10 mL) was

(11) Chen, H.; Bartlett, R. A.; Dias, H. V. R.; Olmstead, M. M.; Power, P. P. *J. Am. Chem. Soc.* **1989**, *111*, 4338.
(12) Ellison, J. J.; Ruhlandt-Senge, K.; Power, P. P. *Angew. Chem., Int. Ed.* **1994**, *33*, 1178.
(13) Ellison, J. J.; Ruhlandt-Senge, K.; Hope, H.; Power, P. P. *Inorg. Chem.* **1995**, *34*, 49.
(14) Wehmschulte, R. J.; Power, P. P. *Organometallics* **1995**, *14*, 3264.
(15) Kays, D. L.; Cowley, A. R. *Chem. Commun.* **2007**, 1053.
(16) Müller, H.; Seidel, W.; Görls, M. *Angew. Chem., Int. Ed.* **1995**, *36*, 325.
(17) Bartlett, R. A.; Power, P. P. *J. Am. Chem. Soc.* **1987**, *109*, 7563.
(18) Au-Yueng, H. Y.; Lam, C. H.; Lam, C.-K.; Ang, W.-Y.; Lee, H. K. *Inorg. Chem.* **2007**, *46*, 7695.
(19) La Pointe, A. M. *Inorg. Chem. Acta.* **2003**, *345*, 359.
(20) Reiff, W. M.; La Pointe, A. M.; Witten, E. H. *J. Am. Chem. Soc.* **2004**, *126*, 10206.
(21) Reiff, W. M.; Schulz, C. E.; Whangbo, M. H.; Seo, J. I.; Lee, Y. S.; Potratz, G. R.; Spicer, C. W.; Girolami, G. S. *J. Am. Chem. Soc.* **2009**, *131*, 404–405.
(22) Pangborn, A. B.; Giardello, M. A.; Grubbs, R. H.; Rosen, R. K.; Timmers, F. J. *Organometallics* **1996**, *15*, 1518.
(23) Tilley, T. D.; Gavenonis, J. *Organometallics* **2000**, *21*, 5549.
(24) Twamley, B.; Hwang, C.-S.; Hardman, N. J.; Power, P. P. *J. Organomet. Chem.* **2000**, *609*, 152.
(25) Ruhlandt-Senge, K.; Ellison, J. J.; Wehmschulte, R. J.; Pauer, F.; Power, P. P. *J. Am. Chem. Soc.* **1993**, *115*, 11353.
(26) Ghosh, A. K.; Bischoff, A.; Cappiello, A. *Eur. J. Org. Chem.* **2003**, 821.

added, and the mixture was stirred and heated to reflux for 5 min to afford a deep-red solution. The solvent was removed under reduced pressure and the entire flask heated from bottom to top at ~180 °C for 5 min. The resulting red solid was extracted with ~100 mL of hexane, filtered via cannula, and left to stand at ambient temperature for 2 d to afford pale-red block-like crystals, yield 0.420 g (39%), mp 248 °C. ^{1}H NMR (300 MHz, C_6D_6, 25 °C) δ 7.10 (br, s, ArH), 2.14 (br, s), 1.20 (br, s), 0.84 (br, s), 0.27 (br, m), −64.3 (br, s). IR, cm^{-1}: ν(N−H) 3340, 3300; ν(Fe−N) tentatively assigned as 340, 315. UV−vis, nm (ε, M^{-1} cm^{-1}): 434 (3880), 322 (13300).

X-ray Crystallography. Crystals of appropriate quality for X-ray diffraction studies were removed from a Schlenk tube under a stream of nitrogen and immediately covered with a thin layer of hydrocarbon oil (Paratone). A suitable crystal was then selected and attached to a glass fiber and quickly placed in a low-temperature stream of nitrogen (90 K).[27] Data for compounds **1** and **2** were obtained on a Bruker SMART 1000 instrument using Mo Kα radiation (λ = 0.71073 Å) in conjunction with a CCD detector. The collected reflections were corrected for Lorentz and polarization effects by using Blessing's method as incorporated into the program SADABS.[28,29] The structures were solved by direct methods and refined with the SHELXTL v.6.1 software package.[30] Refinement was by full-matrix least-squares procedures with all carbon-bound hydrogen atoms included in calculated positions and treated as riding atoms. N-bound hydrogens were located directly from the Fourier difference map.

Magnetic Measurements. DC magnetization measurements were obtained at Northeastern University using a Quantum Design MPMS SQUID magnetometer in applied fields up to 5 T on ~60 mg samples in Quantum Design Delrin holders sealed under nitrogen with Apiezon-N grease.

^{57}Fe Mössbauer Effect Spectroscopy. Zero-field Mössbauer spectra were recorded using a standard constant acceleration spectrometer with an accompanying Janis Vari-Temp Cryostat for temperatures as low as 1.3 K with temperature measurement based on calibrated silicon diodes and vapor pressure thermometry for samples sealed under nitrogen with Devcon Epoxy in cylindrical nylon holders. A 50 mCi (^{57}Co(Rh)) γ-ray source was used for spectral determinations with calibration based on the hyperfine patterns of α-Fe foil (6.5 μm thick) and polycrystalline α-Fe_2O_3. Longitudinal applied field Mössbauer spectra (E_γ parallel to H_0) were obtained using Janis Super Vari-Temp cryostats for magnetic fields up to 9 T (Knox College) and 8 T (Carnegie Mellon University) for complexes **1** and **2**, respectively.

Electron Spin Resonance Spectroscopy. Perpendicular and parallel-polarization continuous-wave electron spin resonance (CW ESR) spectra were recorded using a Bruker ECS106 spectrometer equipped with a dual-mode cavity (ER 4116DM) operating at X-band microwave frequencies. Cryogenic temperatures were achieved and controlled using an Oxford Instruments ESR900 liquid helium cryostat in conjunction with an Oxford Instruments ITC503 temperature and gas flow controller.

DFT Calculations. The electronic structure calculations were performed with the Gaussian 03 program[31] using the hybrid BLYP approximation to the exchange-correlation functional within DFT theory, which was previously shown to perform well for the description of the low-valent iron compounds. The BLYP was combined with a double-ζ quality 6-31g* basis set for most of the optimized geometries. Several truncated models were used for these calculations: models M1 and M2 were based on the X-ray data for linear **1** and bent **2**, respectively, where the alkyl groups on the flanking aryls were replaced with hydrogens. In the models M1′ and M2′ terphenyl ligands were replaced by phenyl groups, while M1″ is simply the (predicted linear) Fe(NHMe)$_2$.

Table 1. Selected Crystallographic Data for Compounds **1** and **2**

cmpd	**1** (linear)	**2** (bent)
formula	$C_{72}H_{100}N_2Fe$	$C_{48}H_{52}N_2Fe$
fw	1049.39	712.77
color, habit	red rod	red block
crystal system	monoclinic	triclinic
space group	$P2_1/n$	$P\bar{1}$
a, Å	12.9432(9)	9.297(2)
b, Å	17.7150(12)	12.066(3)
c, Å	14.6698(10)	18.576(5)
α, deg	90	103.632(4)
β, deg	113.1570(10)	103.712(4)
γ, deg	90	95.549(4)
V, Å^3	3092.6(4)	1941.6(8)
Z	2	2
crystal dim, mm^3	0.42 × 0.38 × 0.22	0.45 × 0.34 × 0.28
T, K	90(2)	90(2)
d_{calc}, g/cm^3	1.127	1.219
abs. coefficient μ, mm^{-1}	0.286	0.424
θ range, deg	1.78 to 27.50	1.17 to 25.25
reflections collected	27551	13646
unique reflections	7087	7009
R(int)	0.0392	0.0353
obs reflections [$I > 2\sigma(I)$]	5324	5586
data/restraints/parameters	7087/0/403	7009/0/530
R_1, observed reflections	0.0442	0.0695
wR_2, all	0.1234	0.1868

Results and Discussion

Synthesis and Structural Characterization. The complexes **1** and **2** were synthesized by a transamination approach that involved the treatment of Fe{N(SiMe$_3$)$_2$}$_2$ with 2 equiv of the appropriate primary arylamine in accordance with eq 1.

$$\mathrm{Fe\{N(SiMe_3)_2\}_2} + 2\mathrm{H_2NAr} \xrightarrow{\Delta} \mathrm{Fe\{N(H)Ar\}_2} + 2\mathrm{HN(SiMe_3)_2} \quad (1)$$

1, Ar = C_6H_3-2,6-(C_6H_2-2,4,6-Pr^i_3)$_2$ (Ar*)

2, Ar = C_6H_3-2,6-(C_6H_2-2,4,6-Me_3)$_2$ (Ar$^{\#}$)

The compounds **1** and **2**, which represent the first examples of stable, homoleptic, primary amides of iron, were isolated as red, crystalline solids. Primary, homoleptic amido {−N(H)R} Fe(II) derivatives were previously unavailable, most likely because the diminished steric protection afforded by a ligand that carries only one organic substituent at nitrogen was insufficient to stabilize such complexes. However, the very large sizes of the Ar$^{\#}$ and Ar* substituents enable monomeric species to be readily isolated. IR spectroscopy revealed absorptions at 3350 (**1**), 3340 (**2**), and 3300 (**2**) cm^{-1}, consistent with the presence of −NH moieties in each complex. Despite several attempts using a 1:1 ratio of reactants at elevated temperature, the imides (FeNAr$^{\#}$)$_n$ or (FeNAr*)$_n$ were not isolated.

X-ray crystallography (see Table 1) showed that both **1** and **2** were well-separated monomers with the closest metal−metal approaches being 11.70 Å for **1** and 9.30 Å for **2**. Complex **1**, Figure 1, has a linear N−Fe−N array with a crystallographically-required inversion center at iron. The strictly linear structure of **1** is unique for an iron(II) amide in the crystalline

(27) Hope, H. *Prog. Inorg. Chem.* **1995**, *41*, 1.
(28) Blessing, R. H. *Acta Crystallogr.* **1995**, *51A*, 33.
(29) Sheldrick, G. M. *SADABS*, version 2.10, Siemens Area Detector Absorption Correction; Universität Göttingen: Göttingen, Germany, 2003.
(30) Sheldrick, G. M. *SHELXTL*, version 6.1; Bruker AXS, Inc.: Madison, WI, 2002.
(31) Frisch, M. J.; et al. *Gaussian 03*, revision A.1; Gaussian, Inc: Pittsburgh, PA, 2003.

Table 2. Important Interatomic Distances (Å) and Angles (deg) for Compounds **1** and **2**

$Fe\{N(H)Ar^*\}_2$ (**1**)			
Fe(1)−N(1)	1.9017(14)	N(1)−Fe(1)−N(1)	180
N(1)−C(1)	1.381(2)	Fe(1)−N(1)−H(1)	117.5(16)
N(1)−H(1)	0.82(2)	C(1)−N(1)−Fe(1)	130.06(11)
Fe(1)−C(7)	2.792	C(1)−N(1)−H(1)	112.4(16)
		N(1)−C(1)−C(2)	119.34(14)
		N(1)−C(1)−C(6)	123.14(14)

$Fe\{N(H)Ar^\#\}_2$ (**2**)			
Fe(1)−N(1)	1.909(3)	N(1)−Fe(1)−N(2)	140.94(16)
Fe(1)−N(2)	1.913(3)	H(1)−N(1)−Fe(1)	116(3)
N(1)−H(1)	1.01(5)	H(2)−N(2)−Fe(1)	114(3)
N(1)−C(1)	1.371(5)	C(1)−N(1)−Fe(1)	128.5(3)
N(2)−H(2)	0.94(5)	C(25)−N(2)−Fe(1)	127.2(3)
N(2)−C(25)	1.368(5)	H(1)−N(1)−C(1)	113(3)
Fe(1)−C(16)	2.690	H(2)−N(2)−C(25)	118(3)
Fe(1)−C(31)	2.588	N(1)−C(1)−C(2)	119.2(3)
		N(1)−C(1)−C(6)	122.2(3)
		N(2)−C(25)−C(26)	118.1(3)
		N(2)−C(25)−C(30)	122.9(4)

phase. In contrast, the N−Fe−N geometry in **2** is bent (Figure 2) with an N−Fe−N angle of ∼141°. There are also apparently weak secondary interactions with the metal center from a flanking ring from each ligand as exemplified by the distances Fe(1)---C(7) = 2.792(1) Å in (**1**) and Fe(1)---C(16) = 2.690(3) Å and Fe(1)---C(31) = 2.588(3) Å in **2** as illustrated by dashed lines in figures 1 and 2. The Fe−N distances in **1** (1.902(1) Å) and **2** (1.911(3) Å, average) may be compared with those previously reported for $Fe\{N(SiMe_2Ph)_2\}_2$ (Fe−N = 1.903(7) Å, N−Fe−N = 172.1(1)°),[11] $Fe\{N(SiMePh_2)_2\}_2$ (Fe−N = 1.917(2) Å, N−Fe−N = 169.0(1)°),[11,17] $Fe\{N(Mes)BMes_2\}_2$ (Fe−N = 1.938(2) Å, N−Fe−N = 166.6(1)°)[7] and $Fe(NBu^t_2)_2$ (Fe−N = 1.879(2) Å, N−Fe−N = 179.45(8)°).[21] Thus, the almost equal Fe−N bond lengths in **1** and **2** lie within the previously known limits. It is also noteworthy that, with the exception of the almost linear $Fe(NBu^t_2)_2$ (note: the silylamide $Fe\{N(SiMe_3)_2\}_2$ is linear in the vapor phase[10a] but is dimerized with three-coordinate irons in the solid[10b]), the three previously observed solid-state structures of two-coordinate iron amides all feature bending of the metal coordination geometry, although we observe that the degree of bending in **2** is ∼20° greater than that previously reported.[4] Thus, it seems probable that the strongly bent geometry in **2** is a result of the lower steric requirement of the Ar# substituent vs Ar*. In the solid state, two-coordinate metal complexes often display deviations from linearity owing to the tendency of the generally electron-deficient metal center (8 valence electrons for Fe(II)) to interact with electron-rich moieties such as flanking aryl groups via bending or dimerization. Bending can be prevented by using very large substituent groups which require the distance between them to be maximized to avoid steric congestion as in linear **1**. With less bulky ligands the substituents can approach each other more closely, and bending becomes allowed as in **2**. Even so, the secondary interactions between the iron and a carbon in **2** (2.690(3) and 2.588(3) Å) are not much shorter than those in **1** (2.79(2) Å) (see Table 2 for interatomic distances and angles for **1** and **2**), and their weakness is emphasized by the fact that they exceed a single Fe−C bond length by ∼0.5−0.6 Å.[14−19]

Magnetism, ESR, and Mössbauer Spectroscopic Data. In view of the linear and significantly bent structures of complexes **1** and **2**, respectively, one has for the first time a unique opportunity to investigate great extremes of orbital magnetism

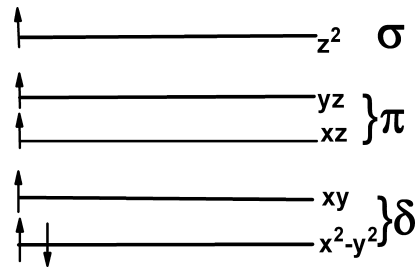

Figure 3. Crystal field splitting diagram (high-spin d^6) showing atomic orbital symmetry labels for ideal homoleptic linear two-coordination.

for an open shell first transition series ion in a common oxidation and spin state, namely high-spin Fe(II), in complexes that carry electronically similar ligands. As **1** is linear, there is no requirement for linear (first-order) Jahn−Teller distortion of its coordination environment.[32] A spontaneous bending distortion (so-called Renner or Renner−Teller effect) can arise from higher-order nonlinear terms in the vibronic coupling[32] and lead to quenching of first-order orbital angular momentum. However, this effect is likely to be somewhat, if not completely, vitiated for the solid state form of two-coordinate complexes with bulky ligands. In any event, these observations and the high degree of coordinative unsaturation lead to the expectation of extraordinary orbital contributions to the effective magnetic moment, isothermal magnetization and internal hyperfine fields of complexes such as **1,** in some cases values broaching those of the corresponding free ion.[20] On the other hand, the bent structure of complex **2** mimics the essential end result of a large Renner Effect distortion, i.e., a sterically allowed (aryl−π)---Fe interaction-driven distortion leading to bending and concomitant partial quenching of orbital magnetism. The orbital ground state of **1** is likely to be intrinsically or at least accidently degenerate in view of the nonbonding, δ symmetry of the ground d_{xy}, $d_{x^2-y^2}$ pair (Figure 3) with respect to the primary amide ligands. This leads to a $\delta^3\pi^2\sigma^1$ ground configuration which is the basis of the $^5\Delta_g$ orbital ground term[33] in local $D_{\infty h}$ symmetry. This ground state exhibits first-order orbital angular momentum owing to the presence of the aforementioned orbital degeneracy and the existence of a rotational symmetry element (C_8, 45° rotation) connecting the d_{xy}, $d_{x^2-y^2}$ pair.[34] The magnetization, ESR, and Mössbauer spectroscopy results that follow confirm that the latter ground state term does indeed lead to (a) very large (first-order) orbital angular momentum and (b) appreciable orbital magnetism in the limit of its spin−orbit splitting, ultimately resulting in a so-called quasi-degenerate spin−orbit[35,36] electronic ground state. Lastly, we partially rationalize our results in terms of DFT calculations for complexes **1** and **2**.

Effective Moments and Isothermal Magnetization. The temperature dependence of the effective moment for the bent complex, **2**, in various applied fields, is presented in Figure 4. It is evident that the effective magnetic moments at ambient temperature range from ∼5.25 to ∼5.80 μ_B. These values for μ_{eff} are near or greater than those normally observed for the

(32) Bersuker, I. B. *Chem. Rev.* **2001**, *101*, 1067.
(33) Wang, S. G.; Schwarz, W. H. E. *J. Chem. Phys.* **1998**, *109*, 7252.
(34) Drago, R. S. *Physical Methods for Chemists*; Harcourt Brace Jovanovich: New York, 1993; p 484.
(35) Pavel, E. G.; Kitajima, N.; Solomon, E. I. *J. Am. Chem. Soc.* **1998**, *120*, 3949.
(36) Andres, H.; Bominar, E. L.; Smith, J. M.; Eckert, N. A.; Holland, P. L.; Münck, E. *J. Am. Chem. Soc.* **2002**, *124*, 3012.

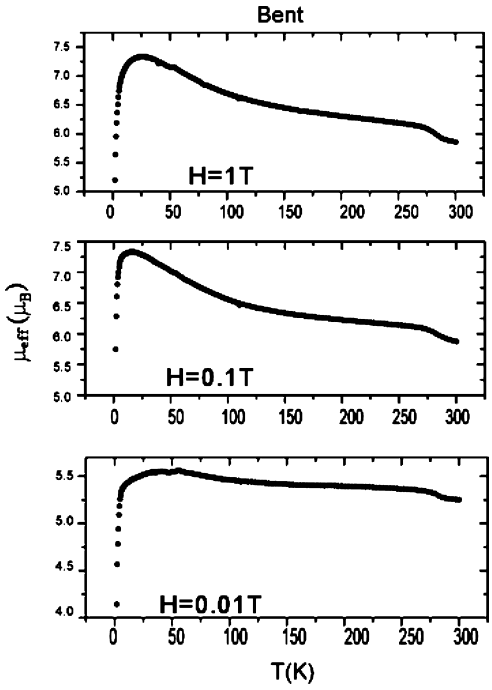

Figure 4. Zero-field-cooled DC temperature dependence of the effective magnetic moment of complex **2** in various applied fields.

upper range of μ_{eff} values for typical high-spin Fe(II).[37] (Recall that spin-only behavior for high-spin Fe(II) corresponds $\mu_{eff} = \sqrt{24}$ or $\sim 4.9\ \mu_B$). We know of no other detailed magnetization studies of genuine linear and/or bent two coordinate high-spin Fe(II) systems save for those on the linear $Fe\{C(SiMe_3)_3\}_2$[20] and the almost linear (N−Fe−N = 179.45(8)°) diamide Fe(N-$Bu^t_2)_2$.[21] Suffice it to say that the effective moment vs temperature profiles of both **1** and **2** are rather reminiscent of those predicted and observed for certain pseudo-octahedral complexes of Fe(II), especially in the limit of a Stevens orbital angular momentum reduction factor, $k \approx 1$, i.e., little or no electron delocalization due to covalency. This is consistent with the σ-bonding anionic nature of the (first short period element) primary amide ligands.[10a] Unoccupied, ligand-centered molecular orbitals are not energetically close to the occupied Fe 3d orbitals, minimizing any nephelauxetic delocalization behavior. The gradual rise in μ_{eff} as T decreases to ~70 K is expected since the greater than half-filled shell d^6 configuration of high-spin Fe(II) requires λ ($\pm\zeta_{3d}/2S$) to be negative (the free ion single electron spin−orbit constant ζ_{3d} for Fe(II) is $\sim 400\ cm^{-1}$). That is, one is progressively populating larger values of J ($= L + S$) at lower temperatures. Finally, at lowest temperatures, the effects of single-ion zero-field splitting appear to predominate, and μ_{eff} decreases.

While complexes **1** and **2** exhibit qualitatively similar magnetization behavior, the magnitude of μ_{eff} as a function of temperature for **1** is ~1.2 to 2.0 μ_B greater than that for **2** (*cf.* Figures 4 and 5). This is consistent with a measurably larger orbital contribution to $\mu_{eff.}$ for the linear complex. Such an observation is not unexpected in view of its linear structure leading to the absence of so-called linear or first-order Jahn−Teller distortion. Figures 4 and 5 clearly show DC field alignment effects for complexes **1** and **2**. This effect is expected to lead to larger limiting μ_{eff} values for **1**, owing in part to its intrinsically larger ground-state orbital angular momentum. These interpretations have much firmer, direct support from consideration of a comparison of the applied field Mössbauer spectra of **1** and **2**, *vide infra*. In passing, we point out a knee in μ_{eff} versus T in the vicinity of 275 K for **2** that is not observed for **1**. This probably suggests a structural phase transformation for **2** although we do not have ambient temperature structures or calorimetry (DSC, etc.) data to pursue this possibility further at this time.

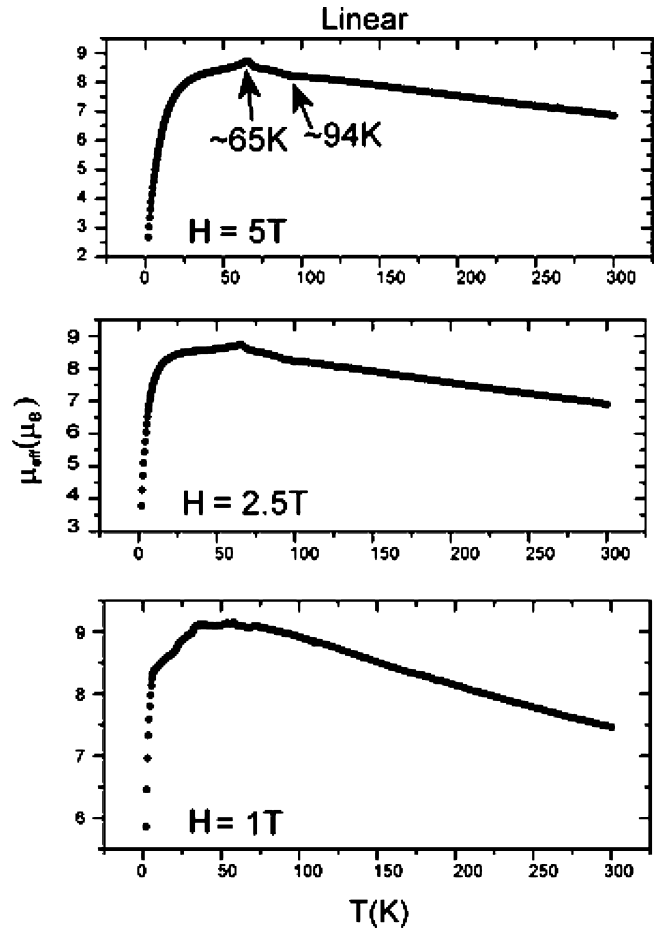

Figure 5. Zero-field cooled DC temperature dependence of the effective magnetic moment of complex **1** in various applied fields. The small irregularities at ~94 and ~64 K are believed to be the result of condensation of dioxygen and antiferromagnetic ordering of the α-dioxygen polymorph contaminant in our SQUID magnetometer.

Figure 6 shows the (field cooled) isothermal magnetization of **1** (top) and **2** (bottom) at 1.8 K. It is apparent that **2** is not saturated at 5 T. This is likely the result of strong local magnetic anisotropy. On the other hand, **1** exhibits a magnetization well in excess of that of the spin-only value for $S = 2$ (22,340 emu/mol). In fact its value is some 96% of the value (27,913 emu/mol) corresponding to an $S = 5/2$ spin-only value. This implies a very large orbital contribution for **1**. In effect, we have an orbital magnetism contribution that is essentially equivalent to adding one full spin unit to the spin-only behavior of high-spin Fe(II). Nevertheless, both **1** and **2** are simple, rapidly relaxing paramagnets (in zero field) where **1** exhibits large first-order orbital contributions to its moment.[38] There is no evidence of long-range cooperative magnetic effects, namely ferromagnetism

(37) Figgis, B. N.; Lewis, J.; Mabbs, F. E.; Webb, G. A. *J. Chem. Soc. A* **1967**, 442.

(38) Kahn, O. *Molecular Magnetism*; VCH-Wiley: New York, 1993; pp 31−52.

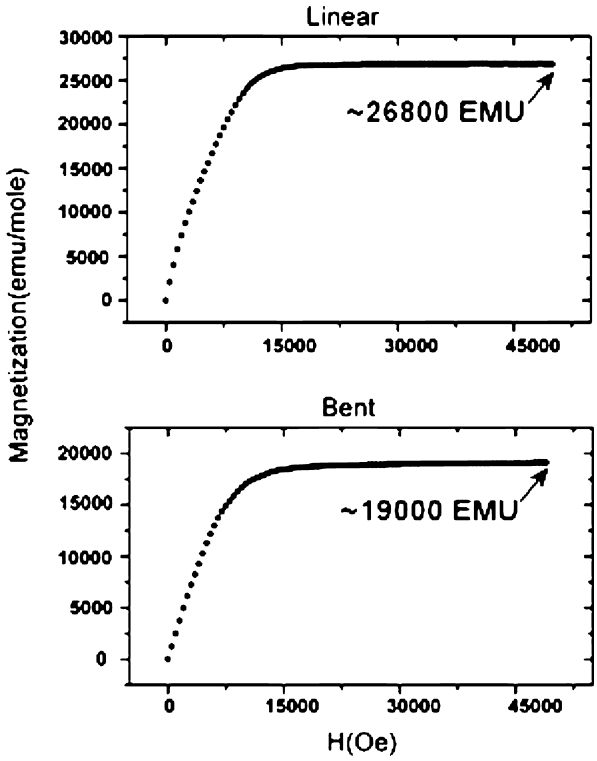

Figure 6. Field-cooled DC magnetization versus applied field at 1.8 K for complexes **1** (top) and **2** (bottom). The spin-only maximum for Fe(II) magnetization is ~22,340 emu.

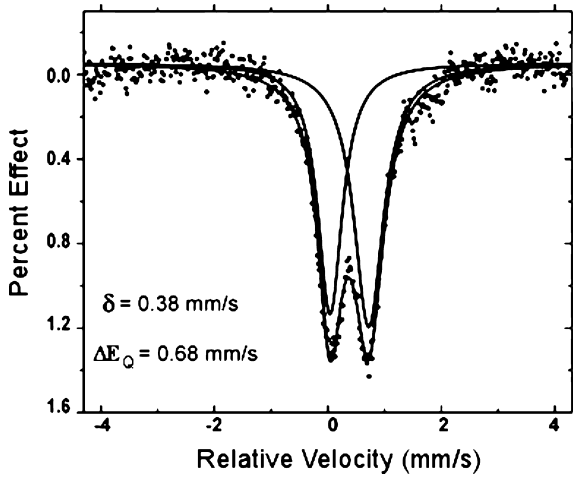

Figure 7. Zero-field Mössbauer spectrum of complex **1** at 293 K.

or canted antiferromagnetism, capable of enhancing the measured magnetic moments (the intermolecular Fe---Fe distances in both compounds exceed 9 Å).

Zero and Applied Magnetic Field Mössbauer Spectroscopy. Complex **1** exhibits a single, quadrupole doublet (Figure 7) in zero field to as low as 4.2 K. This behavior is characteristic of a unique iron environment and rapidly relaxing paramagnetism. At first sight, its small and relatively temperature-independent quadrupole splitting values ($\Delta E_Q = 0.68$ mm/s at 293 K, 0.74 mm/s at 77.5 K and 0.96 mm/s at 20 K), seem atypical of high-spin iron Fe(II), especially when one recalls that the valence shell electron occupation contribution to the z-component of the electric field gradient tensor, $4/7q <r^{-3}>_{3d}$, is large (~3 mm/s) and positive for an electron in either orbital of the ground d_{xy}, $d_{x^2-y^2}$ pair, Figure 3. Apparently, the field gradient tensor

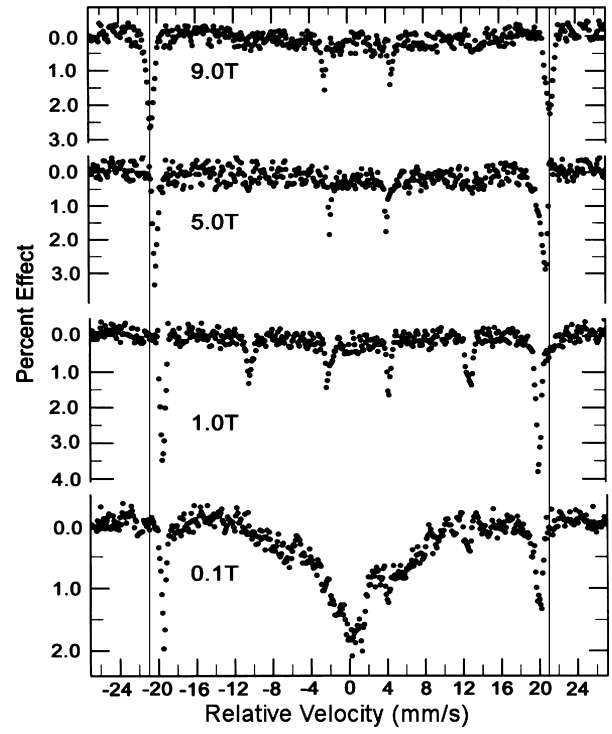

Figure 8. Longitudinal applied field Mössbauer spectra of complex **1** at 4.2 K. Note that the $\Delta m_I = 0$ transitions disappear between 1.0 and 5.0 T.

arising from covalence anisotropy owing to the axially disposed ligands (which should be negative in this case) largely cancels that induced by the occupation of the in-plane 3d orbitals. The isomer shifts of **1** ($\delta = 0.38$ mm/s at 293 K, 0.46 mm/s at 77.5 K, and 0.45 mm/s at 20 K) fit in nicely with the expected decrease in δ with decreasing coordination number for ^{57}Fe of a given spin, oxidation state, and coordination environment. Presently, however, there is an insufficient Mössbauer parameter database for two-coordinate iron from which to make quantitative comparisons.

The application of a magnetic field has a spectacular effect on the Mössbauer spectrum of **1** (Figure 8). The not quite fully resolved nuclear Zeeman splitting apparent in the 0.1 T spectrum (bottom) is diagnostic of slow, but not infinitely slow, electron spin relaxation. The features present at +20 and −19 mm/s indicate that the applied field H_0 of only 1000 gauss causes an effective field H_{eff} at the ^{57}Fe nucleus of some 122 T (1.22 megagauss). This results from slow electron spin relaxation, leading to dramatic Zeeman splitting of the nuclear spin levels. The infinitely slow relaxation limit is essentially reached in the 1 T spectrum and all six (two $\Delta m_I = 0$, two $\Delta m_I = +1$ and two $\Delta m_I = -1$) γ-ray transitions[39] of the typical nuclear Zeeman pattern of ^{57}Fe are clearly evident with H_{eff} now ≈ 124 T. At $H_0 = 5$ T, the two $\Delta m_I = 0$ transitions have all but disappeared. This signifies that the internal field at the iron atoms is now largely polarized parallel to H_0 and E_γ, where E_γ is the electric field component of the incident γ-radiation. At this point, H_{eff} is ~126 T. Finally, at 9 T, one has more or less "complete polarization" of the sample moments and H_{eff} ≈ 130 T. Note that the

(39) Greenwood, N. N.; Gibb, T. C. *Mössbauer Spectroscopy*; Chapman and Hall: London, 1971.
(40) La Macchia, G.; Gagliardi, L.; Power, P. P.; Brynda, M. *J. Am. Chem. Soc.* **2008**, *130*, 5104.

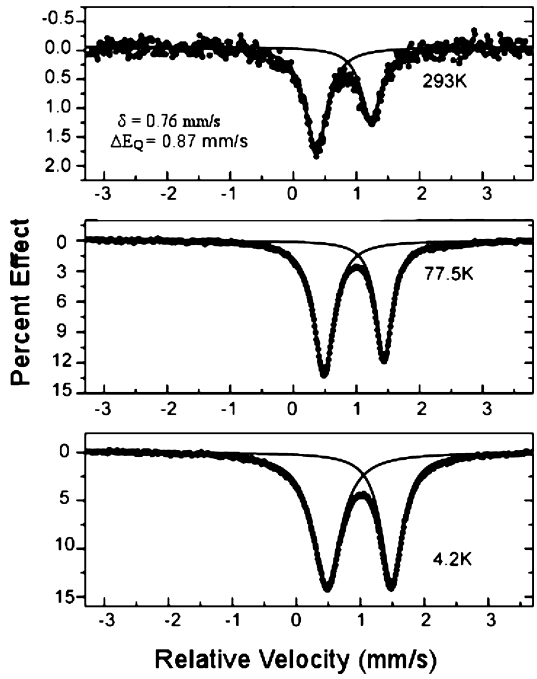

Figure 9. Zero-field Mössbauer spectra of complex **2** at various temperatures.

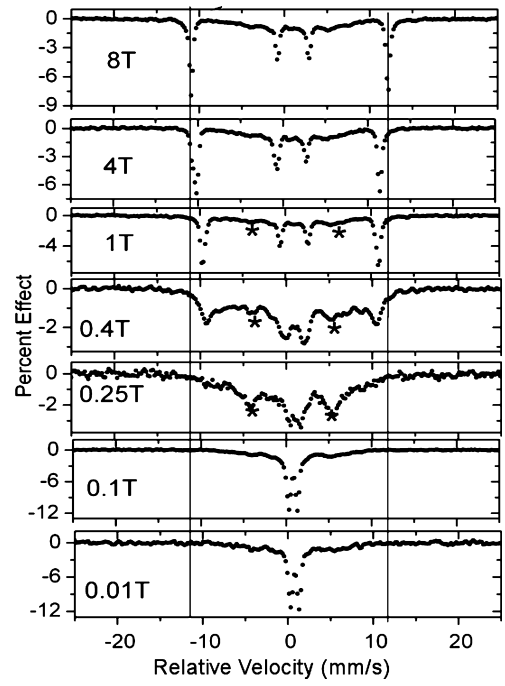

Figure 10. Longitudinal applied field Mössbauer spectra of complex **2** at 4.2 K. The asterisks mark the $\Delta m_I = 0$ nuclear transitions whose intensity diminish beyond 1 T.

effective internal fields have been obtained neglecting any quadrupolar shift of the inner four nuclear γ resonances of the Zeeman pattern relative to the outer two (small in the case of complex **1**). Furthermore, the magnitude of these nuclear splittings has increased monotonically with increasing magnitude of the applied field. This implies that the internal field is positive and that the dominant contribution to this field is the orbital component H_L. The other contributions to the internal hyperfine field are embodied in the equation for the effective field, namely: $H_{eff} = H_0 + H_{internal} = H_0 + H_F + H_D + H_L$ where H_F is the Fermi contact contribution to H_{int} and H_D is the dipolar term. Making reasonable assumptions concerning H_D and H_F as outlined in ref 36, one calculates H_L for complex **1** to be ~170 T (1.70 megagauss). The values for H_{int} and H_L are among the largest ever observed regardless of spin, oxidation state, or coordination environment in all of known iron chemistry to date. To our knowledge, the values of these parameters for **1** are exceeded only by those for the linear two-coordinate complex $Fe\{C(SiMe_3)_3\}_2$[20] for which $H_{int} = 152$ T and $H_L = 203$ T with $H_0 = 0$ at 4.2 K. Without a doubt, the ground state of **1** has an extremely large first-order orbital angular momentum.

The zero-field Mössbauer spectra of bent **2** presented in Figure 9 are noteworthy in that the isomer shifts ($\delta = 0.76$ mm/s at 293 K and 0.95 mm/s at 4.2 K) are markedly larger than for any previously characterized two-coordinate Fe(II) complex. However, these larger δ values are consistent with an increase in the effective coordination number due to weak Fe---C interactions with the flanking aryl rings on the amide ligand (Figure 2, dashed lines). The local symmetry of the coordination environment (with or without the proposed flanking interactions) is at most C_{2v}. This is a point group whose irreducible representations are all unidimensional and thus nondegenerate. Hence, the bending leads to the expectation of a measurable quenching of first-order orbital angular momentum relative to complex **1**. Essentially, this is confirmed by the applied field Mössbauer spectra of complex **2** (Figure 10) that are now considered. The sequence of Figure 8 is roughly reproduced in Figure 10 except that the field resolution is higher. The asterisks of Figure 10 correspond to the two $\Delta m_I = 0$ transitions which have all but disappeared at 1 T. We note that there is some impurity background absorption evident in the spectra, especially at 8 T. However, this does not interfere with the interpretation that follows.

It is clear that the internal field of **2** is positive again as for complex **1** indicating a dominant orbital contribution. However at $H_0 = 8$ T, the value of H_{eff} is ~73 T from which one calculates $H_L = 116$ T. This represents a ~32% decrease in orbital angular momentum (using the H_L value as a metric) relative to complex **1**, a large but by no means total quenching of L. In fact in the context of orbital angular momentum, the behavior of the bent complex **2** (N−Fe−N angle = 141°) is reminiscent of that of a series of planar three-coordinate (C_{2v}) ferrous complexes of reference 36. Specifically, the CH_3-substituted Fe(II) β-diketiminate analogue (N−Fe−N = ~95°) in the series has an internal field of 82 T. This corresponds to $H_L \approx 133$ T (neglecting H_D) where the authors interpret the large internal field in terms of mixing of closely spaced or accidentally degenerate ground state d orbitals via spin−orbit coupling. This leads to a quasi-degenerate electronic ground state with near maximal orbital angular momentum for the particular ground state d orbital pair involved, namely (d_{z^2}, d_{yz}) in the three coordinate iron series. Note, however, that while this system is somewhat similar to **2** of this work, neither has a first-order contribution to L. Referring to Figure 3, the ground state orbital (d_{xy}, $d_{x^2-y^2}$) pair of complex **1** is degenerate or at least accidentally so and is likely to be similarly accidently degenerate in **2** owing to their nonbonding δ symmetry in the present linear and bent systems. However, there is no longer a very large first-order contribution in **2** since in C_{2v} the $C_8(45°)$ rotational symmetry element that transforms d_{xy} to $d_{x^2-y^2}$ or vice versa is lost. One can, however, invoke the aforementioned spin−orbit coupling "unquenching" mechanism of reference 36

Table 3. Comparison of H_L Values for Different Symmetries

complex	local symmetry	orbital field H_L (Tesla)	formal symmetry	ref
Fe{C(SiMe$_3$)$_3$}$_2$	$D_{\infty h}$	203	D_{3d}	20
1	$D_{\infty h}$	170	C_{2h}	this work
Fe{N(Bu^t)$_2$}$_2$	$D_{\infty h}$	155	D_2	21
(β-diketiminato)Fe-CH$_3$	C_{2v}	133	C_{2v}	36
2	C_{2v}	116	C_2	this work

for **2**. It is likely that the similarity of the orbital magnetism of **2** to that of the three-coordinate C_{2v} β-diketiminate complexes of reference 36 is not coincidental.

In summary, strictly speaking, the electronic ground states of linear two-coordinate ferrous complexes are better considered either as (i) a pure spin−orbit doublet ($m_J = \pm 4$ arising from the ground J state for the ^{5}D term of Fe(II))[20] or (ii) such a doublet mixed to varying degrees (in lower symmetry) with nearby adjacent spin−orbit states where the extent of mixing depends on the prevailing symmetry of the complex. This contention arises, in the context of perturbation theory, from the facts that (a) we have minimal ligation with only two relatively weak field anions, and (b) the spin−orbit coupling perturbation to the Hamiltonian $\mathbf{H} = \lambda LS$ is near maximal owing to the approach of L to 2. In any event, (i) should lead to ESR silence and infinitely slow paramagnetic relaxation in $H_0 = 0$. Only an absence of rhombic ZFS will lead to true ESR silence if D is greater than the energy of the microwave quantum. Specifically, the zero-rhombicity Fe{C(SiMe$_3$)$_3$}$_2$[20] is ESR silent out to 26 T at 4.2 K and exhibits fully resolved magnetic hyperfine splitting of its zero-field Mössbauer spectrum up to ~50 K.[41] Its uniaxial magnetism and extraordinary internal hyperfine field have been adequately explained in terms of an isolated pure $m_J = \pm 4$ ground state.[42] The ground state described in situation (ii) ensures a degree of "allowedness" to ESR transitions but will require an externally applied magnetic field (albeit usually relatively small) in order to induce slow paramagnetic relaxation and resolved hyperfine splitting of Mössbauer spectra, and where H_L is expected to be reduced somewhat, owing to the mixing. This is the case for complex **1** of this work and the diamide system Fe(NBu$^t_2$)$_2$.[21] In this light, it is instructive to consider Table 3, especially the first three entries wherein it is seen that the value of H_L is qualitatively quite sensitive to the overall (formal) symmetry of the complex even for the $D_{\infty h}$ entries. However, while tantalizing, the unequivocal confirmation of the importance of such secondary (formal) symmetry considerations clearly demands the study of numerous other linear and bent two-coordinate complexes of high-spin Fe(II).

ESR Spectroscopy. The 4.2 K parallel-polarization CW ESR spectra (Figure 11, top) of the linear and bent Fe(II) amido complexes are typical of those for high-spin ferrous ($S = 2$) compounds wherein the zero-field splitting (Δ) of the $m_s = \pm 2$ doublet is less than the energy of the incident microwave photon ($h\nu = 0.314$ cm^{-1} for 9.42 GHz radiation). The effective g-values (11.22 and 11.60) measured at the point where the spectrum crosses the zero-line for duplicate preparations of **1** and **2**, respectively, are significantly greater than the spin-only g-value of 8. This is again diagnostic of large orbital angular momentum in the electronic ground state achieved either by orbital degeneracy of the ground state (as expected for high-symmetry molecules)[20] or spin−orbit coupling (usually in the case of heavier element complexes). The ESR studies of **1** and **2** are thus more or less in harmony with the magnetic studies discussed above. That the CW ESR spectrum of the bent Fe(II) amido complex **2** is much broader than that for the linear complex **1** is likely due to more pronounced D-strain, i.e., structural inhomogeneity leading to a distribution of zero-field splitting values. This hypothesis is also supported by the X-ray structural data for **2** which shows greater thermal atomic motion than that in **1** (*cf.* thermal ellipsoids in Figures 1 and 2). As described earlier,[43] the field position for the $|2, +2\rangle \leftrightarrow |2, -2\rangle$ transition is a function of Δ which itself can be related to the axial (D) and rhombic (E) terms of the zero-field splitting tensor $\hat{H} = D[\hat{S}_z^2 - 2 + (E)/(D)(\hat{S}_x^2 - \hat{S}_y^2)]$. Small structural changes give rise to different values for D and E, altering the field position (B_0) that meets the resonance condition and thus broadening the EPR line.

The shift of the uniaxial g-value, g_z from the free-electron value (2.0023) scales linearly with the expectation value of orbital angular momentum operator $\langle L_z \rangle$ in the electronic ground state. Using literature formulas, the approximations given in ref 36 and the values for H_L determined from our Mössbauer studies, we compute $\langle L_z \rangle = 8.8\kappa$ for **1** and 6.8κ for complex **2**, where κ is dimensionless constant related to the Fe s orbital contribution to the description of the ground state (usually $0.2 < \kappa < 0.4$). If we assume κ for both complexes is the same (a fair assumption based on the similarity of the coordinating ligands) then clearly g_z should be larger for complex **1**. However, in the parallel-mode EPR experiment, the resonant condition is met when $\sqrt{\Delta^2 + (4g_z\beta B_z)^2} = h\nu$, where $\Delta = 3D(E/D)^2$. Thus, depending on the exact values for the principal elements of the ZFS tensor, the effective g-value for complex **2** could be larger than that for complex **1**. Indeed, as it is considerably bent away from axial symmetry, we expect E/D to be relatively large for complex **2**.

On the other hand, we note that the effective g-values derived from the 10 mM (and repeated at 1 mM) frozen toluene solution ESR spectra (Figure 11) may indeed not be fully consistent with the magnetization and Mössbauer spectroscopy results for the neat, undiluted polycrystalline solids. Needless to say, both types of data clearly suggest large orbital contributions for **1** and **2**. However, the g_{eff}-value for the bent complex is larger than that of the linear analogue. In the absence of other data (primarily frozen solution applied field Mössbauer spectra for Fe^{57} enriched versions of **1** and **2**), we speculate that, though unlikely, this result may suggest linearity for **2** in frozen solution owing to different packing effects for the frozen solution versus the neat polycrystalline solid.

DFT Calculations. The gas phase optimized structural parameters for M1 and M2, models based on the X-ray coordinates of **1** and **2** with their alkyl groups replaced by hydrogens, given in Table 4 reproduce most of the experimental bond lengths and bond angles reasonably well, *cf.* Table 2. The differences of a few degrees in the optimized and experimental N−Fe−N and C−Fe−N angles are most probably due to packing effects (which are always present with the large terphenyl ligands) that are not taken into account in the optimized gas phase structure. The quintet state was determined to be lowest in energy for both complexes by computing various spin states for M1 and M2,

(41) Reiff, W. M. Unpublished results for Fe{C(SiMe$_3$)$_3$}$_2$.
(42) Dadi, D.; Whangbo, M. H. *Inorg. Chem.* **2005**, *44*, 4407.
(43) Surerus, K. K.; Hendrich, M. P.; Christie, P. D.; Rottgardt, D.; Orme-Johnson, W. H.; Münck, E. *J. Am. Chem. Soc.* **1992**, *114*, 8579.

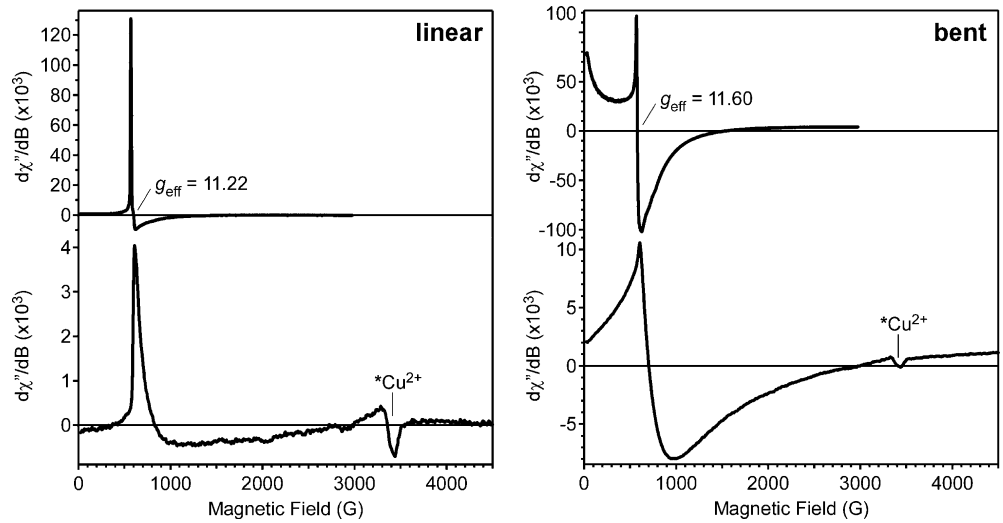

Figure 11. Parallel ($h\nu$ = 9.42 GHz, top) and perpendicular ($h\nu$ = 9.69 GHz, bottom) polarization CW ESR spectra of 0.01 M toluene solutions of linear **1** (left) and bent **2** (right) at 4.2 K. Modulation amplitude = 10 G, frequency = 100 kHz, time constant = 20.48 ms, conversion time = 40.96 ms, microwave power = 0.2 mW.

Table 4. Selected Optimized Geometrical Parameters (B3LYP/6-31g(d)) for the M1 and M2 Models, Which Have the Naked Terphenyl C_6H_3-2,6-Ph_2 as the Ar Substituent on Each Nitrogen Atom[a]

	Fe−N	N−C_{ipso}	N−Fe−N	Fe−N−C_{ipso}
M1	1.908	1.386	180.0	130.8
(**1**)	(1.902)	(1.381)	(180.0)	(130.1)
M2	1.912	1.385	143.9	123.9
(**2**)	(1.909, 1.913)	(1.369,1.370)	(140.9)	(128.5, 127.2)

[a] Experimental values from X-ray data are given in parentheses.

Table 5. Computed Energy (au) for the Quintet, Triplet and Singlet Spin States of Model Compounds[a]

	singlet	triplet	quintet
Fe(NHC_6H_3-2,6-Ph_2)$_2$, M1	−2747.30735	−2747.35606	−2747.41009
Fe(NHC_6H_3-2,6-Ph_2)$_2$, M2	−2747.40512	−2747.45210	−2747.50300
Fe$(NHPh)_2$, M1′	−1828.20480	−1828.26796	−1828.31774
Fe$(NHPh)_2$, M2′	−1828.28989	−1828.34892	−1828.40143

[a] Structures were applied from X-ray data to the linear M1 and bent M2 models (C_6H_3-2,6-Ph_2 as the Ar substituent) and to M1′ and M2′ (Ph as the Ar substituent).

and for M1′ and M2′, simpler models with the Ar* and Ar# on nitrogen replaced by Ph. The corresponding energies are listed in Table 5. Calculations were also carried out on the M1/M2 system where the N−Fe−N angle was varied from 145 to 180°. The corresponding curves for triplet and quintet spin states are illustrated in Figure 12. The quintet ground state lies 33.9 kcal/mol lower than the triplet and 64.5 kcal/mol lower than the singlet state for the linear model. For the bent model the corresponding energy differences are 31.0 and 61.4 kcal/mol, respectively.

The electronic structures of **1** and **2** are similar, with the exception of some interactions between the flanking aryl orbitals and metal-centered orbitals that occur mainly in the bent form, and are weaker and more distant in the linear form. The breaking of symmetry from a linear to a bent structure has the effect of slightly increasing the HOMO−LUMO gap (68.3 kcal/mol for the linear and 77.6 kcal/mol for the bent structure).

In order to further check whether the quintet ground state of the iron amide obtained from DFT exhibits some multiconfigurational

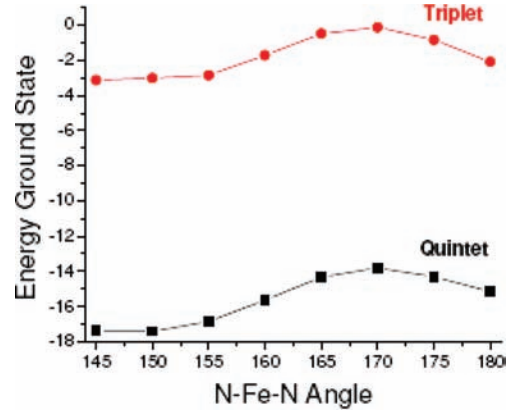

Figure 12. Relative energies (au) computed for triplet and quintet spin states by varying the N−Fe−N angle in M1/M2 from 145° to 180°.

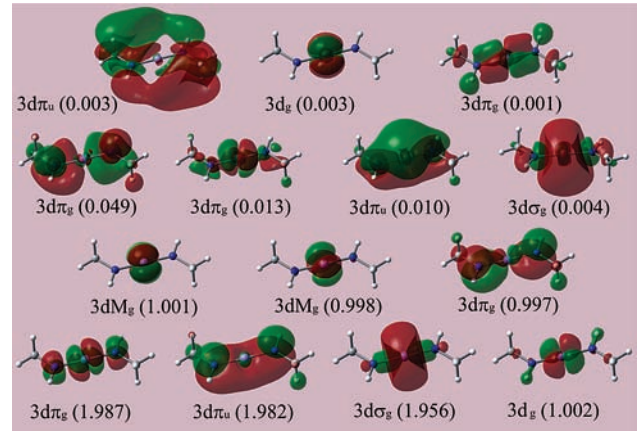

Figure 13. CAS orbitals for the model Fe{N(H)Me}$_2$ (M1″), predicted to be linear, with the corresponding occupation numbers. The designation M indicates a metal localized orbital.

character, we have performed a CASSCF calculation on the linear model M1" (in which the Ar* or Ar# are replaced by a methyl group) using Alhrichs double-ζ basis set with one polarization function. Linear geometry was predicted to be a potential minimum for this model. A total of 10 electrons were included in 14 active

orbitals, resulting in overall 1249248 configurations. The computed occupation numbers illustrate the bonding, in which three unpaired electrons are located in d_{zy}, d_{xy} and $d_{x^2-y^2}$ metal-centered orbitals and the fourth unpaired electron resides in a nominally bonding orbital composed of iron d_{xz} and two p_x AO's of nitrogen (Figure 13). For the active space selected, the quintet ground state is highly monodeterminant, as evidenced by the weight of the leading CAS configuration (0.976) interaction of the Fe d_{xz} orbital with the p_z AO's of nitrogen, an interaction which is symmetry forbidden in the linear form of this compound. Finally, the spin density is very similar in both cases and is almost exclusively centered at the metal. A small spin delocalization is observed in both cases on the nearby nitrogen atoms, but no delocalization onto the aryl ligands occurs.

It is clear that the DFT calculations are in very good agreement with the experimental data. Most importantly, a ground-state quintet is proven to be the most stable in both linear and bent structures. Furthermore, the unpaired electrons are localized for the most part in the iron d-orbitals such that they can provide the very large orbital moment in a linear geometry.

Conclusion

The main finding of the experimental and theoretical results in this paper is that the very large first-order orbital angular momentum associated with the sterically fixed linear coordination geometry of the Fe(II) ion in **1** is due to the absence of first-order Jahn−and Renner−Teller distortion effects that normally lift ground-state electronic degeneracy. Thus, the orbital angular momentum is greatly diminished by simple bending to a nonlinear form. A direct comparison of this type was previously unavailable and is here permitted for the first time by the steric adaptability of the terphenyl amide ligands.

Acknowledgment. We are grateful to the National Science Foundation (Grant CHE-0641020) for financial support. W.M.R. is grateful for partial support by the NSF Division of Materials Research for the purchase of a SQUID magnetometer at Northeastern University. He also thanks Professor Eckard Münck (Carnegie-Mellon University) for informative discussions and applied field Mössbauer spectra of complex **2**. The work in the laboratory of R.D.B. is supported by the National Institutes of Health (Grant GM 48242).

Supporting Information Available: X-ray crystallographic data for **1** and **2**, further information on the DFT calculations, and complete ref 31.This material is available free of charge via the Internet at http://pubs.acs.org.

JA903439T